Revealing the nebular properties and Wolf-Rayet population of IC10 with Gemini/GMOS

Katie Tehrani,[1]* Paul A. Crowther,[1] I. Archer[1]

[1]*Department of Physics and Astronomy, University of Sheffield, Sheffield, S3 7RH, UK*

ABSTRACT

We present a deep imaging and spectroscopic survey of the Local Group irregular galaxy IC10 using Gemini North and GMOS to unveil its global Wolf-Rayet (WR) population. We obtain a star formation rate (SFR) of 0.045 ± 0.023 $M_\odot yr^{-1}$, for IC10 from the nebular Hα luminosity, which is comparable to the SMC. We also present a revised nebular oxygen abundance of $\log(O/H) + 12 = 8.40 \pm 0.04$, comparable to the LMC. It has previously been suggested that for IC10 to follow the WR subtype-metallicity dependance seen in other Local Group galaxies, a large WN population awaits discovery. Our search revealed 3 new WN stars, and 6 candidates awaiting confirmation, providing little evidence to support this claim. The new global WR star total of 29 stars is consistent with the LMC population when scaled to the reduced SFR of IC10. For spectroscopically confirmed WR stars, the WC/WN ratio is lowered to 1.0, however including all potential candidates, and assuming those unconfirmed to be WN stars, would reduce the ratio to ~0.7. We attribute the high WC/WN ratio to the high star formation surface density of IC10 relative to the Magellanic Clouds, which enhances the frequency of high mass stars capable of producing WC stars.

Key words: stars: Wolf-Rayet – galaxies: individual (IC10) – ISM: abundances

1 INTRODUCTION

IC10 is a barred irregular galaxy in the Local Group, considered by some as a blue compact dwarf (Richer et al. 2001). Situated beyond the plane of the Milky Way ($b=-3.3°$), attempts to study this galaxy are hindered by a high galactic foreground reddening of E(B-V) = 0.77 (Richer et al. 2001). With recent distance determinations ranging from 660 kpc (Gonçalves et al. 2012) to 817 kpc (Sanna et al. 2008), we adopt an IC10 distance of 740 $\pm$ 20 kpc[1]. McConnachie (2012) derived a stellar mass of 7.5×10^7 $M_\odot$ for IC10, an order of magnitude lower than the Small Magellanic Cloud (SMC). IC10 is gas rich with an atomic hydrogen content of 4.4×10^7 $M_\odot$, adjusted to our adopted distance. The galaxy is also metal-poor, with an oxygen abundance measurement of $\log(O/H) + 12 = 8.26$ (Garnett 1990). This metallicity is intermediate between those of the Magellanic Clouds, making them good comparative galaxies.

The recent star formation history of IC10 is very uncertain. Studies of the neutral hydrogen content by Wilcots

& Miller (1998) revealed that the gas distribution has been shaped by stellar winds rather than supernovae explosions, suggesting the observed interstellar medium features are relatively young. From this it was suggested that the galaxy is currently undergoing a starburst episode which began approximately 10 million years ago. The current star formation rate was found to be 0.07 $M_\odot yr^{-1}$ by Gregory et al. (1996), which again is between those of the Magellanic Clouds (Kennicutt et al. 2008). The star formation intensity however, is much greater than both at 0.049 $M_\odot yr^{-1}$ kpc^{-2} (Crowther & Bibby 2009), due to the small physical size of IC10.

Wolf Rayet (WR) stars are post main sequence massive stars progressing through the helium-burning stages of stellar evolution. These stars are dominated by strong winds and high mass loss rates during which they are stripped of their hydrogen, and sometimes helium, envelopes. This distinction lends itself nicely to the criteria for two WR spectral types, the nitrogen sequence (WN) and the carbon sequence (WC), both of which can be divided into further ionization subclasses. The two spectral types are thought to be linked through an evolutionary chain known as the Conti scenario which has since been adapted by Crowther (2007) to take into consideration initial stellar mass.

Narrow-band photometry is useful for identifying potential WR candidates, because the strong winds associated with these stars manifest as broad emission line features

---

* k.tehrani@sheffield.ac.uk

[1] Taken from an average of four different methods; RR Lyrae 820 $\pm$ 80 kpc (Sanna et al. 2008), PNLF 660 $\pm$ 25 kpc (Gonçalves et al. 2012), tip of the Red Giant Branch 740 $\pm$ 60 kpc and Cepheids 740 $\pm$ 60 kpc (Tully et al. 2013).

within the stellar spectrum. Matching narrow-band filters with the emission line wavelengths helps to reveal these stars, especially in crowded environments. This method alone however, is not sufficient to confirm a WR star, or to classify a spectral type. Instead confirmation requires spectroscopy in order to calculate the relevant emission line ratios outlined in Smith et al. (1996) for WN stars, and in Crowther et al. (1998) for WC stars.

Previous surveys of IC10 have been successful at finding WR stars within this galaxy despite the high foreground extinction. Massey et al. (1992) first began the search after suspecting a large population of massive stars would be likely when considering the number of H II regions identified within the galaxy (Hodge & Lee 1990). Further studies such as Massey & Armandroff (1995); Royer et al. (2001); Massey & Holmes (2002); Crowther et al. (2003) led to the confirmation of 26 WR stars, hereafter referred to as M#, and R# depending on which collaboration initially identified the candidate. The discovery of these WR stars was curious. Not only does IC10 now have the highest surface density of WR stars in the Local Group, the ratio of WC/WN spectral types does not agree with that expected from evolution models for a galaxy of such a low metallicity.

Currently the WC/WN ratio stands at 1.3, which is an order of magnitude higher than other metal poor star forming galaxies such as the LMC (0.2) and SMC (0.1) (Breysacher et al. 1999; Neugent et al. 2012a; Massey et al. 2014, 2015b; Foellmi et al. 2003a). It has been proposed that either an unusual starburst has occurred, or there are further WN stars residing unnoticed within IC10 (Massey & Holmes 2002). Therefore, to confidently verify the WR content of IC10 we must first be satisfied the search is complete, especially in the context of the recent discovery of unusually faint WN stars in the LMC (Massey et al. 2014; Neugent et al. 2017).

The purpose of our study therefore, is to use deep narrow-band imaging to establish if a hidden population of WR stars is a plausible explanation for the apparently abnormal WC/WN ratio. Since the metallicity of IC10 is intermediate between the LMC and SMC, we also look to compare the properties of WR stars found in each galaxy. Finally we aim to identify the fraction of IC10 WR stars residing in binary systems. The new photometric and spectroscopic data to achieve these aims are presented in Sect. 2. Sect. 3 focuses on the results from nebular emission including an update of the metallicity and star formation rate (SFR). In Sect. 4 we present the stellar results from these observations, a discussion of these results in Sect. 5, and brief conclusions in Sect. 6.

2   OBSERVATIONS.

2.1   Imaging

We obtained deep imaging observations of IC10 on the 24 September 2009 using the GMOS instrument (Hook et al. 2004) on the 8m Gemini North telescope at Mauna Kea (ID GN-2009B-Q-9, PI Crowther). Due to the emission line nature of WR stars, narrow-band filters are more suited to identify potential candidates, therefore four narrow-band filters and one broadband filter were selected, with details outlined in Table 1. Two of the narrow-band filters were centred

Table 1. Characteristics of the five filters used with GMOS and the imaging quality of IC10

Filter	λ_c [nm]	FWHM [nm]	T_{exp} [s]	FWHM ['']
He II	468	8	3 x 1750	0.59
He IIC	478	8	3 x 1750	0.56
Hα	656	7	3 x 60	0.53
HαC	662	6	3 x 60	0.52
g	475	154	3 x 30	0.59

on strong emission lines, and the remaining two were continuum filters, denoted by the suffix C. The He II 4686 emission line is particularly strong within all WR subtypes, therefore to identify He II excess candidates both continuum and emission-line imaging is necessary. The $330'' \times 330''$ field of view on GMOS-N is composed of three CCDs separated by a $2.8''$ gap. To compensate for this gap, IC10 was observed three times through each filter, with each subsequent image shifted by $5''$. The resultant field of view can be seen in the colour composite image shown in Fig. 1, where the positions of all confirmed WR stars have also been highlighted.

Images in the same filter were aligned and combined in IRAF before using the DAOPHOT package to find the relative magnitudes of all sources with an appropriate point spread function (Stetson 1987). To convert narrow-band values to apparent magnitudes a zero point correction was applied, derived from observations of the standard star BD +28 4211.

We also obtained broad g-band imaging which was reduced using a similar method, however standard star observations were unavailable. Instead, isolated sources were selected from within the GMOS field of view for which apparent magnitudes were obtained from PanSTARRS1 g-band observations (Chambers et al. 2016). These standard stars provided an average g-band zero point correction for the remainder of the GMOS data.

Of the 37 previous WR candidate stars, 36 were located and identified within our field of view. The exception, M22, had previously been dismissed as a potential WR by Massey & Armandroff (1995), and of the 37 candidates, 26 have been confirmed as WR stars. Photometric results for confirmed WR stars are shown in Table 2 where positions have been astrometrically corrected based on PanSTARRS data. New WR candidates were selected from a combination of image subtraction techniques, blinking of the He II and He IIC images, and quantitative relative magnitude comparisons to reveal an excess of He II 4686 emission. A visual inspection of all HeII excess sources with a greater than 3 sigma detection was completed to remove spurious sources, and 11 new emission candidates were revealed with their photometric properties outlined in Table A1 in the appendix. We note that T8 appears extended with FWHM measurements of $0.64'' \times 0.98''$, compared to the average FWHM of $0.66'' \times 0.63''$ for point sources. We therefore advise that although this source exhibits a HeII excess it is unlikely to be confirmed a WR star. Fig. 3 shows the He II excesses as a function of continuum magnitude for the potential WR candidates, along with a comparison including all DAOPHOT sources.

Fig. 2 shows the logarithmic number count distribu-
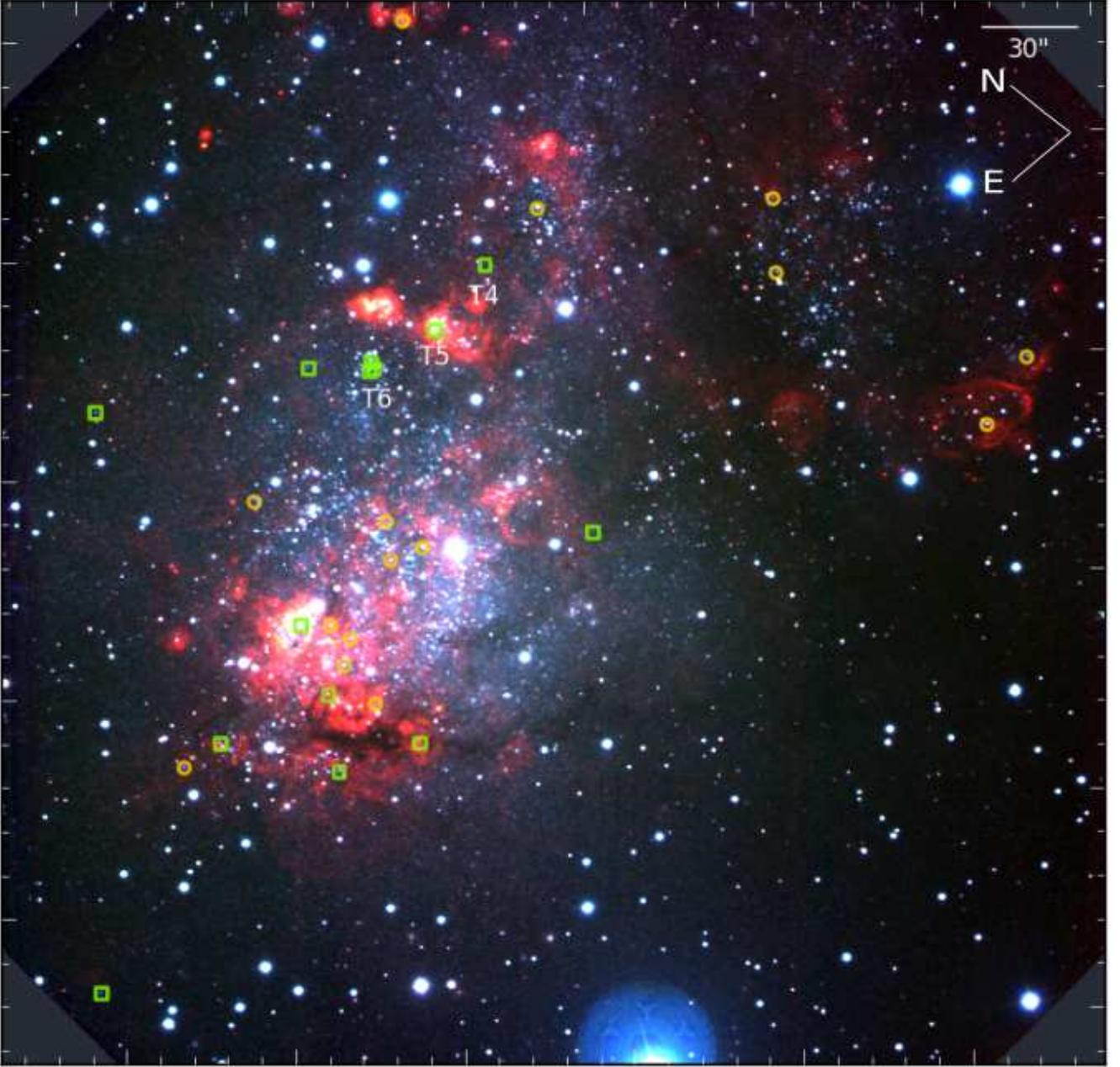
Figure 1. Gemini GMOS colour composite image of IC10 showing the relative positions of previously confirmed WN stars (green squares) and WC stars (yellow circles), with the 3 new WN stars labelled. Field of view shown in image is $300'' \times 314''$, corresponding to 1.1×1.1 kpc at a distance of 740 kpc. RGB image generated from red-H$\alpha(\lambda 656nm)$, green-g($\lambda 475nm$), and blue-He II($\lambda 468nm$) filter images.

tion of He IIC magnitudes across all sources located by DAOPHOT within our field of view with a least squares polynomial fit applied to the region in which this relationship is linear. The point at which this relationship breaks down, and the slope turns over indicates the faintest magnitude we consider this survey to be complete to within a 3σ error, which for He IIC corresponds to an apparent magnitude of 25.3 mag. Using the same principle for the He II photometry results in a faint magnitude limit of 24.7 mag. From our compiled list of 11 WR candidates, two fall outside this completeness limit (T3 and T8).

The He IIC apparent magnitude was corrected for interstellar extinction using an average E(B-V) of 0.92, discussed in Sect. 4.3, so A_{4780}=3.4 mag when adopting A_{4780}/A_V=1.194 from the Galactic extinction law (Seaton 1979). We adopt a distance modulus of 24.3 $\pm$ 0.07 mag, corresponding to a distance of 740 $\pm$ 20 kpc, and from that we reach an absolute magnitude survey limit of -2.4 mag for the He II continuum.
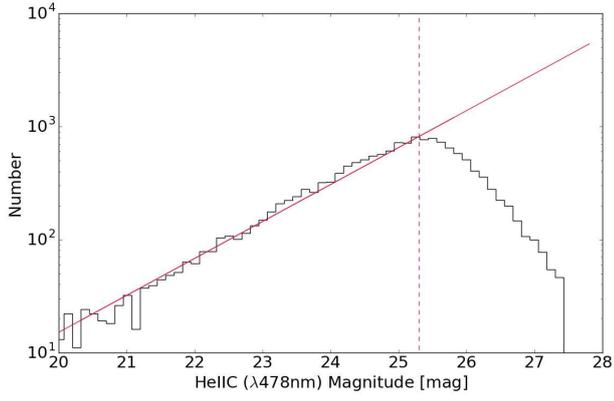
Figure 2. Logarithmic histogram showing the He ɪɪC(λ478nm) mag for all sources within the field of view. The peak of the curve indicates this survey is complete to an apparent He ɪɪC magnitude of 25.3, or absolute magnitude of -2.4 for an adopted E(B-V)=0.917, A_{4780}=1.194 A_V=3.50 and distance modulus of 24.3 mag.
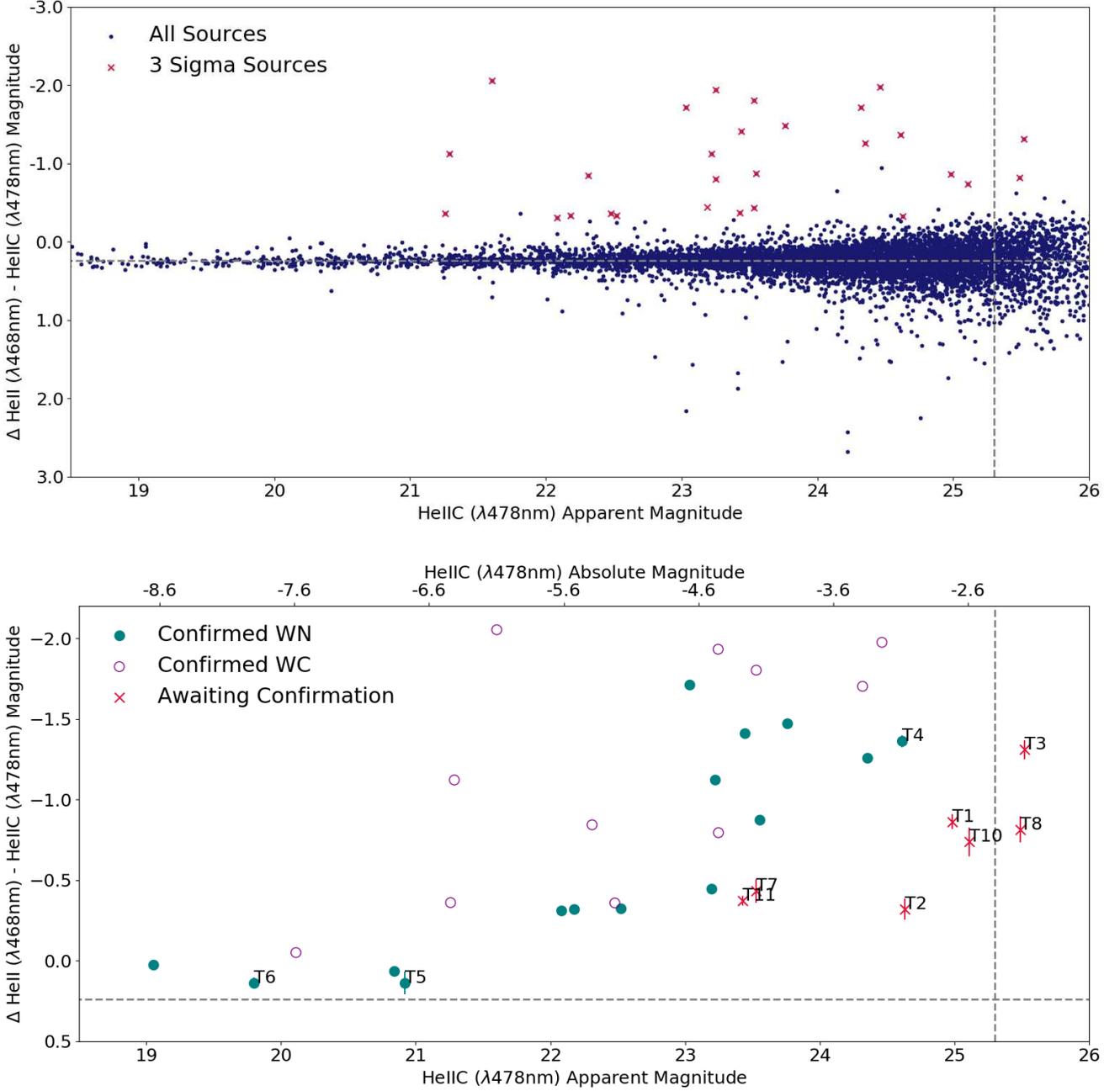
Figure 3. Upper panel shows the relationship between continuum magnitude and He II 4686 excess magnitude for all sources identified by DAOPHOT in IRAF. The He II emission zero-point lies at -0.24, as shown by the horizontal dashed line, due to the high extinction towards IC10. The vertical dashed line corresponds to the survey limit. The majority lie below the zero-excess line indicating no He II emission line excess, and a considerable proportion of the data points are also below the detection limits of this survey, therefore too faint to be considered robust. The red crosses correspond to sources which were found to have a He II detection greater than 3σ. The lower panel is restricted to confirmed WR candidates (WN - closed green circles, WC - open purple circles) and those awaiting confirmation (red crosses). Note that the majority of unconfirmed candidates are much fainter than others in the sample, and there are no candidates included which exceed our He IIC survey limit of 25.3 mag. Both apparent magnitude and absolute magnitudes axis are shown, with absolute magnitudes derived from A_{4780}=3.39 mag and a distance modulus of 24.3 mag.

Table 2. Photometric magnitudes taken from GMOS narrow-band filter images of all currently confirmed WR stars residing within IC10, listed in increasing RA order. HL# refers to the H II region each star is associated with, outlined in Hodge & Lee (1990). Old spectral types are taken from Massey & Armandroff (1995); Royer et al. (2001); Massey & Holmes (2002); Crowther et al. (2003). New spectral classes have been determined from GMOS spectroscopic data (discussed in Sect. 4.1). Interstellar extinction magnitudes were derived using method outlined in Sect. 4.3 using both photometric data shown here and spectral classifications. M_v absolute v-band magnitudes are derived from spectroscopically measured magnitudes and an adopted distance of 0.74Mpc.

ID	HL	RA Dec [J2000]	Old Spectral Type	ref	New Spectral Type	He II [mag]	He IIC [mag]	Hα [mag]	HαC [mag]	g [mag]	E(B-V) [mag]	M_v [mag]
M1	2/3	00:19:56.96 59:17:07.6	WC4-5	c	WC4-5	21.624 ± 0.024		21.028 ± 0.047	21.597 ± 0.019	21.560 ± 0.037	*0.92 ± 0.26*	-5.62 ± 0.87
M2	6	00:19:59.62 59:16:54.7	WC4	c	WC4	21.235 ± 0.020		19.908 ± 0.053	20.764 ± 0.050		*0.92 ± 0.26*	-5.86 ± 0.87
R6	10	00:20:02.99 59:18:26.9	WC4	c	WC4	22.453 ± 0.014	23.248 ± 0.020	20.723 ± 0.033	21.690 ± 0.041	22.441 ± 0.022	1.28 ± 0.04	-5.75 ± 0.14
R5		00:20:04.27 59:18:06.2	WC4-5	c	WC4-5	22.120 ± 0.027	22.479 ± 0.026	20.951 ± 0.035	21.346 ± 0.036	21.822 ± 0.024	0.94 ± 0.04	-5.36 ± 0.14
M4		00:20:11.55 59:18:57.6	WC4-5	c	WC4-5	20.060 ± 0.007	20.111 ± 0.005	18.718 ± 0.007	19.169 ± 0.011	19.510 ± 0.006	0.91 ± 0.01	-7.67 ± 0.07
M5	29	00:20:12.83 59:20:08.0	WNE/C4	c	WNE/C4	21.323 ± 0.008	23.035 ± 0.008	19.665 ± 0.062	21.783 ± 0.032	21.804 ± 0.027	1.04 ± 0.03	-4.86 ± 0.11
T4		00:20:14.47 59:18:49.9			WNE	23.249 ± 0.016	24.612 ± 0.034	22.765 ± 0.123	23.377 ± 0.121	23.958 ± 0.093	1.03 ± 0.10	-3.48 ± 0.35
R13		00:20:15.62 59:17:21.4	WN5	c	WN5	23.092 ± 0.018	24.351 ± 0.025	22.238 ± 0.063	23.306 ± 0.136	23.662 ± 0.061	0.81 ± 0.11	-3.04 ± 0.38
T5	45	00:20:17.43 59:18:39.2			WNE	21.054 ± 0.044	20.918 ± 0.054		19.532 ± 0.069		1.27 ± 0.07	-8.41 ± 0.25
R9	60	00:20:20.31 59:18:39.5	WNE	c	WNE	21.854 ± 0.020	22.176 ± 0.011	20.572 ± 0.022	21.225 ± 0.022	21.412 ± 0.024	0.80 ± 0.02	-4.94 ± 0.09
T6	60	00:20:20.34 59:18:37.3			WNE	19.939 ± 0.019	19.801 ± 0.027	18.125 ± 0.022	18.561 ± 0.018	19.222 ± 0.018	1.15 ± 0.03	-9.15 ± 0.11
R8	60	00:20:20.55 59:18:37.1	WN10	c	WN10	20.903 ± 0.010	20.839 ± 0.015	18.308 ± 0.012	19.714 ± 0.020	20.191 ± 0.009	0.80 ± 0.02	-6.37 ± 0.09
M7	66	00:20:21.95 59:17:41.0	WC4-5	c	WC4-5	20.033 ± 0.017			20.887 ± 0.049		*0.92 ± 0.26*	-6.80 ± 0.87
M9		00:20:22.67 59:18:46.6	WN3	c	WN3	22.284 ± 0.007	23.758 ± 0.013	21.622 ± 0.026	22.822 ± 0.065	22.969 ± 0.030	0.79 ± 0.05	-3.24 ± 0.19
R11	(71)	00:20:22.74 59:17:53.2	WC4	c	WC4	22.615 ± 0.012	24.318 ± 0.030			23.385 ± 0.064	*0.92 ± 0.26*	-2.71 ± 0.87
M10		00:20:23.31 59:17:42.0	WC7	c	WC7	19.548 ± 0.010	21.602 ± 0.011	19.261 ± 0.013	20.012 ± 0.017	20.481 ± 0.007	1.26 ± 0.02	-7.03 ± 0.09
R12	97	00:20:25.65 59:16:48.1	WNE	c	WNE	22.677 ± 0.016	23.552 ± 0.017	20.251 ± 0.041	21.920 ± 0.041	22.587 ± 0.025	1.34 ± 0.04	-5.44 ± 0.14
M12	100	00:20:26.19 59:17:26.2	WC4	c	WC4	21.466 ± 0.014	22.310 ± 0.010	19.858 ± 0.052	20.302 ± 0.039	21.256 ± 0.028	1.63 ± 0.03	-8.09 ± 0.13
R10	106	00:20:26.51 59:17:04.9	WC4	c	WC4	22.486 ± 0.014	24.462 ± 0.027	19.115 ± 0.081		22.726 ± 0.049	*0.92 ± 0.26*	-2.31 ± 0.87
M13	111	00:20:26.66 59:17:32.6	WC5-6	c	WC5-6	20.898 ± 0.012	21.259 ± 0.009	19.903 ± 0.036	20.577 ± 0.020	20.713 ± 0.014	0.59 ± 0.02	-5.22 ± 0.09
M14	(111)	00:20:26.90 59:17:19.7	WC5	c	WC5	20.165 ± 0.007	21.287 ± 0.006	20.266 ± 0.059	20.117 ± 0.025	20.569 ± 0.008	0.97 ± 0.02	-6.59 ± 0.09
M15		00:20:27.06 59:18:17.4	WC6-7	a	WC4	21.726 ± 0.006	23.529 ± 0.031	21.672 ± 0.044	22.923 ± 0.079	22.477 ± 0.021	0.53 ± 0.07	-3.04 ± 0.24
M24	111c	00:20:27.70 59:17:37.1	WN/OB	c	O2.5 If/WN6	19.077 ± 0.019	19.052 ± 0.020	18.240 ± 0.039	18.438 ± 0.022	18.486 ± 0.014	0.65 ± 0.02	-8.36 ± 0.10
R2	(106/115)	00:20:28.03 59:17:14.1	WN7-8	c	WN7-8	21.770 ± 0.013	22.083 ± 0.012	19.834 ± 0.013	20.867 ± 0.013	21.477 ± 0.016	0.97 ± 0.01	-5.98 ± 0.08
M17		00:20:29.09 59:16:51.7	WNE +BH	c	WNE +BH	22.747 ± 0.012	23.194 ± 0.011	22.164 ± 0.098	22.119 ± 0.034	22.590 ± 0.031	0.90 ± 0.03	-5.66 ± 0.12
M19		00:20:31.04 59:19:04.5	WN4	c	WN4	22.095 ± 0.007	23.220 ± 0.011	21.288 ± 0.025	22.616 ± 0.055	22.467 ± 0.018	0.53 ± 0.05	-3.28 ± 0.17
M23	139	00:20:32.76 59:17:16.2	WN7-8	b	WN7	22.195 ± 0.009	22.521 ± 0.014	19.432 ± 0.022	20.164 ± 0.010	21.660 ± 0.013	*0.92 ± 0.26*	-5.41 ± 0.87
M20		00:20:34.49 59:17:14.4	WC5	c	WC5	21.313 ± 0.005	23.246 ± 0.014	21.153 ± 0.031	22.186 ± 0.042	22.223 ± 0.013	0.88 ± 0.04	-4.62 ± 0.14
M21		00:20:41.62 59:16:24.4	WN4	c	WN4	22.031 ± 0.007	23.445 ± 0.017	21.262 ± 0.021	22.424 ± 0.033	22.666 ± 0.023	0.86 ± 0.03	-4.21 ± 0.12

Parentheses around HL regions indicate the WR star is in the close vicinity of, but not necessarily within, the H II region in question.

Italics denote a WR star with an E(B-V) value derived from an average, rather than individually calculated (see Sect. 4.3).

Note the minor revisions to the spectral type of M15 - updated from WC6-7 (Massey & Armandroff 1995), M23 - updated from WN7-8, and M24 - updated from WN/OB (Massey & Holmes 2002; Crowther et al. 2003).

References as follows: a: Massey & Armandroff (1995); b: Massey & Holmes (2002); c: Crowther et al. (2003);

Table 3. Properties of the IC10 masks used with GMOS instrument for multi-object spectroscopy, where mask 1 and 2 correspond to the most recent data set and mask 3 and 4 are from Crowther et al. (2003). For all cases the slit length was set at 5″.

Mask	Slit Width [″]	Observation Date	FWHM [″]
1	0.75	10 Sept 2010	0.5
2	0.75	10 Sept 2010 - 11 Sept 2010	0.6
3	0.8	22 Dec 2001 - 16 Jan 2002	0.7
4	0.8	22 Dec 2001 - 15 Jan 2002	0.8

2.2 Spectroscopy

We obtained follow-up spectroscopic observations, which took place on 10-11 September 2010, again using GMOS on Gemini-North with the program ID GN-2010B-Q-44 (PI Crowther). Two masks were constructed, (mask 1 and 2), each containing 20 targets, with their properties detailed in Table 3. Of the 9 potential candidates identified in Table A1, four were included (T4,T5,T6 and T9) across the two masks.

Four exposures per mask were obtained, each for a duration of 2600s. A slit width was fixed at 0.75″ and the B600 grating was used in all cases, and the spectral resolution of the data was found to be 3.4 Å from arc lines. To compensate for the gaps present in the GMOS detector, the central wavelength was shifted by 20nm from 510nm to 530nm for one pair of exposures for each mask. Signal to noise was improved by merging the four exposures per target, and targets common to both masks were also combined.

Wavelength calibration was completed using an internal CuAr arc lamp, and for the flux calibration, the white dwarf star G191B2B was observed through the same B600 grating with a slit width of 0.75″. Total integration time was 3×30s with a shift in central wavelength between exposures from 410nm, 510nm, and 610nm to ensure the generated response function covered the necessary wavelength range. Slit loss corrections were also applied from photometric magnitudes.

This data set was combined with previous GMOS observations, GN-2001B-Q-20 (mask 3) and GN-2001B-Q-23 (mask 4), which were obtained between 21 December 2001 and 16 January 2002 (Crowther et al. 2003) (see Table 3). Those WR observed in multiple masks underwent further merging to produce a single spectra for each candidate.

3 NEBULAR RESULTS

3.1 Nebular Extinction

A number of spectra within the datasets exhibited prominent nebular emission, prompting a separate analysis to investigate the gaseous properties of IC10. Known H II regions were identified using the maps produced by Hodge & Lee (1990), and we also include data from candidate H II regions suggested by P. Royer (private communication). Table 4 shows which regions were included and provides an overview of the available emission line fluxes measured for each region, relative to Hβ = 100.

Individual reddening corrections, based on Balmer emission line ratios, were computed for each H II region. Depending on the available wavelength range, Hα/Hβ or

Hγ/Hβ ratios were used in conjunction with an intrinsic intensity ratio to obtain a measure of c(Hβ). Observed emission flux measurements were corrected for underlying stellar absorption using:

$$f_{\lambda corr} = f_0 \frac{W_\lambda + W_{abs}}{W_\lambda}$$

where f_0 refers to the observed flux, $f_{\lambda corr}$ is the corrected flux and values for W_{abs} were taken from González Delgado et al. (1999), for an instantaneous burst with Salpeter IMF, mass range of 1-80 M$_\odot$ and age of 2 Myrs. By interpolating between varying metallicity intervals, the W_{abs} parameter was determined to be 2.5Å , 2.4Å and 2.5Å for Hα, Hβ and Hγ respectively. Measured equivalent widths (W_λ) for all Balmer emission lines are included in Table B1 in the Appendix.

The corrected fluxes were then used with:

$$\frac{f_{\lambda corr}}{f_{\beta corr}} = \frac{I_\lambda}{I_\beta} 10^{c(H\beta)[X_\lambda - X_\beta]}$$

where $X_{H\alpha}$, $X_{H\beta}$ and $X_{H\gamma}$ are 0.82, 1.17 and 1.32 respectively, determined from a Galactic extinction law (Seaton 1979), and the intrinsic intensity ratios are $\frac{I(H\alpha)}{I(H\beta)}$=2.86 and $\frac{I(H\gamma)}{I(H\beta)}$=0.47. Table 4 shows the derived c(Hβ) measurements for each H II region, which when combined give an average nebular extinction of c(Hβ)=1.19 $\pm$ 0.28, or E(B-V) $\sim$ 0.7c(Hβ) = 0.83 $\pm$ 0.20. Schlafly & Finkbeiner (2011) find the Milky Way foreground contribution in the direction of IC10 to be E(B-V)=1.39, however note the low galactic latitude of the galaxy translated to a highly uncertain extinction estimate.

3.2 Metallicity

Metallicity measurements are important for providing information about the local environment, and the star formation history of the galaxy. A previous metallicity determination for two H II regions, IC10-1 and IC10-2, outlined by Lequeux et al. (1979) and later catalogued as HL111 and HL45 respectively (Hodge & Lee 1990), suggested oxygen abundance measurements of log(O/H) + 12 = 8.17 and log(O/H) + 12 = 8.45 respectively. Unfortunately the quality of the [O III] 4363 intensity measurement was flagged as uncertain. Garnett (1990) performed a second analysis of HL45, obtaining a metallicity of log(O/H) + 12 = 8.26, again based on the observations from Lequeux et al. (1979). Richer et al. (2001) also report metallicity measurements for the H II regions HL111b and HL111c located within the IC10-1 region and find log(O/H) + 12 = 7.84 and log(O/H) + 12 = 8.23 respectively. These results are summarised in Table 6.

Using the nebular emission present in the regions outlined in Table 4, oxygen abundance measurements based on strong line methods using the N2 and O3N2 ratios from Pettini & Pagel (2004) were determined and are shown in Table 5. Unfortunately, the linear relationship between oxygen abundance and the O3N2 ratio only holds true for O3N2 measurements within the range of -1 to 1.9, and for IC10 our measured O3N2 ratios suggest we are at the limit of this calibration beyond which this linear relationship breaks down. Nevertheless, using our O3N2 ratio we find an average metallicity of log(O/H) + 12 = 8.14 $\pm$ 0.09, with a systematic uncertainty from the method of 0.25. For completeness

Table 4. Nebular emission line flux measurements relative to Hβ=100 for various H II regions. HL# refer to H II regions outlined by Hodge & Lee (1990) and H II# refer to candidate H II regions suggested by Royer et al. (2001). Final column indicates the reddening correction derived for that region using Balmer emission line ratios as described in the text.

Nebular Region	Mask	[O II] 3727	Hγ 4340	[O III] 4363	Hβ 4861	[O III] 4959	[O III] 5007	[N II] 6548	Hα 6562	[N II] 6584	10^{-17} $F_{H\beta}$ [erg cm^{-2} s^{-1}]	c(Hβ)
HL 6	2				100 ± 17	251 ± 22	801 ± 25	64 ± 15	1035 ± 16	172 ± 15	1.89 ± 0.31	1.06
HL 10	2				100 ± 8	64 ± 8	217 ± 9	41 ± 8	1117 ± 11	117 ± 8	2.51 ± 0.21	1.53
HL 20	3		39 ± 4		100 ± 5			33 ± 6	960 ± 8	72 ± 6	16 ± 0.76	1.29
HL 22	4				100 ± 1	116 ± 3	350 ± 3	9 ± 4	640 ± 5	26 ± 4	109 ± 0.89	0.99
HL 45	3				100 ± 1	174 ± 2	508 ± 3	10 ± 3	628 ± 3	29 ± 3	45 ± 1.1	0.96
HL 45	1	21 ± 1	26 ± 0.2	2.2 ± 0.2	100 ± 2	222 ± 2					381 ± 5.8	1.62
H II 04	4		42 ± 5		100 ± 3	115 ± 3	367 ± 4		555 ± 31	27 ± 23	6.56 ± 0.21	0.61
H II 07	3		30 ± 3		100 ± 1	135 ± 2	449 ± 3	10 ± 3	731 ± 3	28 ± 3	127 ± 1.71	1.18
H II 07	4				100 ± 3	132 ± 2	413 ± 3	11 ± 3	719 ± 4	36 ± 3	137 ± 3.72	1.16
H II 08	3				100 ± 1	135 ± 1	428 ± 2	13 ± 3	809 ± 3	42 ± 3	148 ± 0.80	1.31
H II 08	4	41 ± 2	29 ± 0.4		100 ± 1	141 ± 1	439 ± 2				213 ± 2.83	1.36
H II 11	3		7 ± 1		100 ± 2	150 ± 6	500 ± 7	37 ± 5	2041 ± 7	113 ± 5	22 ± 0.36	-

RA and DEC (J2000) co-ordinates for Royer et al. (2001) H II regions as follows: H II 04 (00:20:15.48, +59:18:40.6) H II 07 (00:20:18.51, +59:17:40.4) H II 08 (00:20:24.41, +59:16:55.2) H II 11 (00:20:19.36, +59:18:02.9)

Table 5. Oxygen abundance measurements for H II regions within IC10, derived using the N2 and O3N2 strong line methods outlined in Pettini & Pagel (2004)

Nebular Region	Mask	N2	log(O/H) + 12	O3N2	log(O/H) + 12
HL 6	2	-0.78	8.46 ± 0.41	1.68	8.19 ± 0.26
HL 10	2	-0.98	8.34 ± 0.41	1.32	8.31 ± 0.26
HL 22	4	-1.39	8.11 ± 0.42	1.93	8.11 ± 0.26
HL 45	3	-1.34	8.14 ± 0.41	2.04	8.08 ± 0.25
H II 04	4	-1.31	8.15 ± 0.55	1.87	8.13 ± 0.45
H II 07	3	-1.42	8.09 ± 0.41	2.07	8.07 ± 0.25
H II 07	4	-1.31	8.16 ± 0.41	1.92	8.11 ± 0.25
H II 08	3	-1.29	8.17 ± 0.41	1.92	8.12 ± 0.25
H II 11	3	-1.26	8.18 ± 0.41	1.96	8.10 ± 0.25

we also compute oxygen abundance measurements using the N2 ratio, for which we find log(O/H) + 12 = 8.22 ± 0.14, however we note that the N2 method produces results with a large dispersion, therefore introducing a systematic uncertainty on the metallicity of ± 0.41.

To produce a more robust determination of the oxygen content we also derive an updated metallicity measurement for IC10 using the nebular emission spectra of the newly confirmed WR star T5, which is associated with the HL45 H II region (Hodge & Lee 1990) and is shown in Fig. 4. Whilst nebular emission was present in a number of spectra, solely T5 provided a robust [O III] 4363 flux measurement, as shown in Table 4, necessary when calculating metallicity using the direct T_e method.

HL45 was corrected for an extinction of c(Hβ)=1.62 ± 0.05 found using the method outlined in Sect. 3.1 before appropriate emission line intensities were measured. An [O III] electron temperature of 9700±250 K was found using the nebular package in IRAF, and the same temperature was adopted for the [O II] gas temperature. This approximation should be sufficient since the contribution from the [O III] region dominates the final oxygen abundance measurement,

as shown in Table 6. A change in ± 1000K in [O II] gas temperature corresponds to a ± 0.03 adjustment in log(O/H) + 12.

Assuming a density of 100 cm^{-3} gave an oxygen abundance of log(O/H) + 12 = 8.40 ± 0.04. Present results are included in Table 6. It is apparent that our updated oxygen abundance for HL 45 is similar to Lequeux et al. (1979) although is somewhat higher than both Garnett (1990) and Richer et al. (2001). We consider this oxygen measurement to be a good representation of the global metallicity of IC10 because the oxygen content distribution for other dwarf galaxies has been shown to be relatively uniform. Integral field studies of blue compact dwarf (BCD) galaxies (García-Lorenzo et al. 2008; Cairós et al. 2015) find that for a BCD with a metallicity greater than 8.1, the variation in log(O/H) + 12 across the galaxy does not exceed ∼0.1 dex. A slightly higher metallicity for IC10 is still consistent with the luminosity-metallicity relationship from Shi et al. (2005) for $M_B = -16.3$ mag[2]. The oxygen content of this galaxy is therefore more similar to the LMC (log(O/H) + 12 = 8.37) than the SMC (log(O/H) + 12 = 8.13), and IC10 is not as metal-poor as previously considered.

3.3 Star Formation Rate

Using the Hα and HαC imaging discussed in Sect. 2.1 we also re-determine the star formation rate (SFR) of IC10. Fig. 5 shows the Hα image of IC10, and we include the positions of known WR stars for reference. Using aperture photometry to obtain a total Hα count rate, we apply a conversion derived from standard star measurements to find the integrated Hα flux. A similar exercise for the HαC filter permits the stellar contribution to be subtracted. This approach was

---

[2] Absolute blue magnitude for IC10 obtained from $m_B = 11.8$ mag, $A_B = 4.1 \times$ E(B-V) = 3.8 mag and a distance modulus of 24.3 mag.
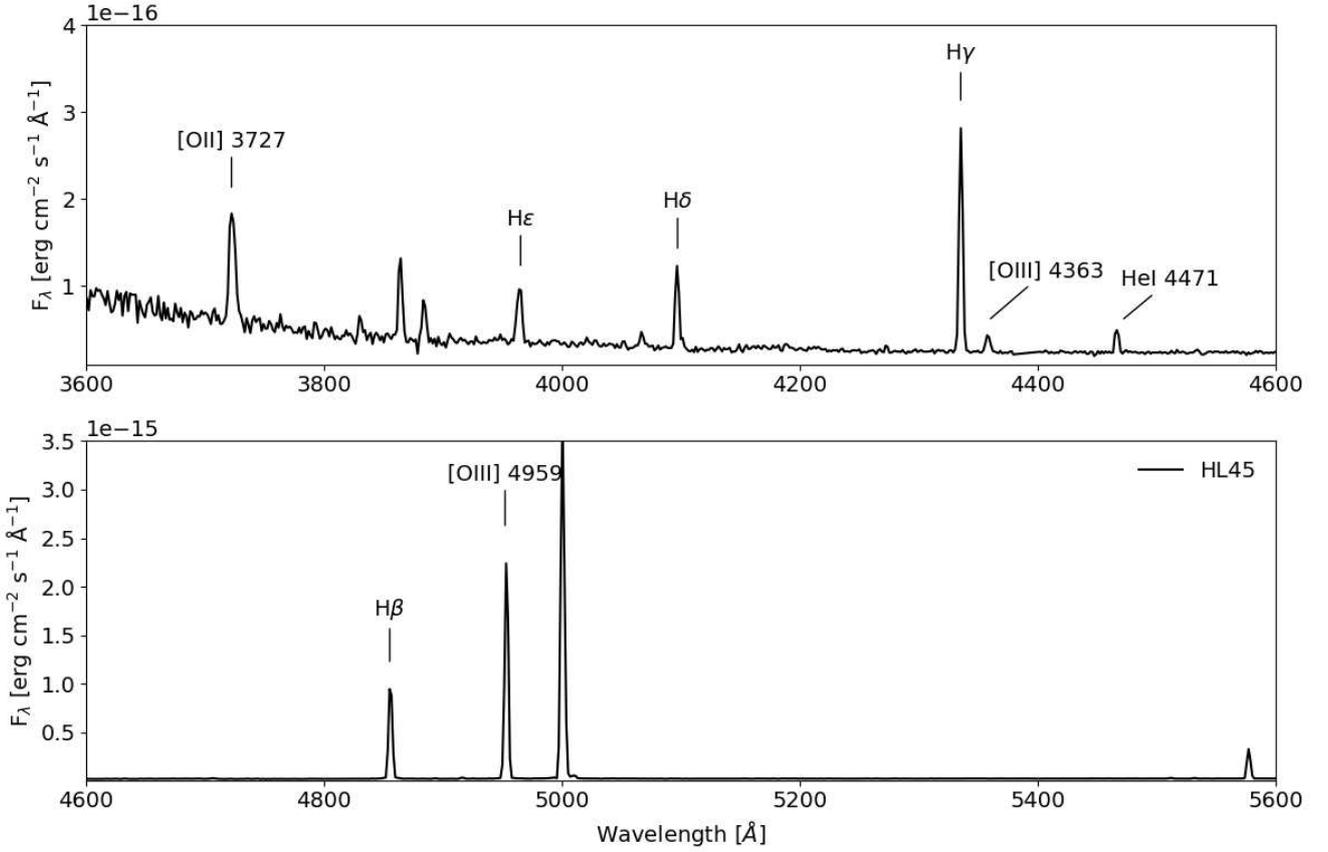
Figure 4. Flux calibrated optical nebular spectra of the H II region HL45, associated with the WR star T5. Labels highlight the Balmer series and other forbidden lines important for metallicity measurements, including a clear [O III] 4363 emission line.

Table 6. Overview of previously derived [O III] temperatures and metallicity measurements for two different H II regions within IC10 (IC10 1 and IC10 2), outlined by Lequeux et al. (1979), and present results from mask1 observations of HL45

Lequeux Region	HL	$T(O^{2+})$ [$\times 10^4$ K]	(O^+/H) [$\times 10^5$]	(O^{2+}/H) [$\times 10^4$]	log(O/H) + 12	Ref
IC10 1	111	1.16	3.98	1.10	8.17	a
IC10 1	111b	1.40 ± 0.30			7.84 ± 0.25	b
IC10 1	111c	1.00 ± 0.06			8.23 ± 0.09	b
IC10 2	45	1.06	6.03	2.19	8.45	a
IC10 2	45	1.08			8.26 ± 0.10	c
IC10 2	45	0.97 ± 0.03	2.28 ± 0.19	2.30 ± 0.21	8.40 ± 0.04	d

a: Lequeux et al. (1979); b: Richer et al. (2001); c: Garnett (1990); d: This work;

preferred to producing a net Hα - HαC image, which introduced subtraction artefacts due to bright stars within the field of view. To correct for [N II] emission included within the GMOS Hα filter bandwidth, we apply the correction:

$$\frac{F([N\,II]6548+6584)}{F(H\alpha)} = 0.09 \pm 0.02$$

derived from average flux measurements of the [N II] 6548, [N II] 6584 and Hα emission lines across all available H II regions (shown in Table 7).

The average gas extinction of c(Hβ)=1.19 ± 0.28 was applied and adopting a distance of 740 ± 20 kpc we find $L_{H\alpha}$=5.64 ± 2.93×10^{39} erg s^{-1}. To convert this to a SFR we use:

$$SFR = 7.94 \times 10^{-42} L_{H\alpha}$$

which assumes a Salpeter function IMF over a mass range of 0.1-100 M$_\odot$, and resulted in a SFR=0.045 ± 0.023 M$_\odot$yr^{-1} (Kennicutt 1998). We also derive a SFR for the dominant giant H II region of IC10 comprising the complex centred on HL111/106 (Hodge & Lee 1990). An elliptical aperture with semi-major/minor axes of 17″× 27″reveals a Hα luminosity of 1.4×10^{39} erg s^{-1}, typical of the brightest H II regions of local star forming galaxies (Kennicutt 1988). These results are shown in Table 10.

A summary of the current and previous SFR determinations, using both Hα and radio flux measurements, are shown in Table 7. Kennicutt et al. (2008) find a lower SFR using a similar method, owing to a lower Hα flux and smaller dust extinction correction. In contrast, our SFR lies intermediate between the radio derived SFRs by Gregory et al. (1996) and Chyży et al. (2016). The comparison to radio derived SFRs is useful because at these wavelengths dust
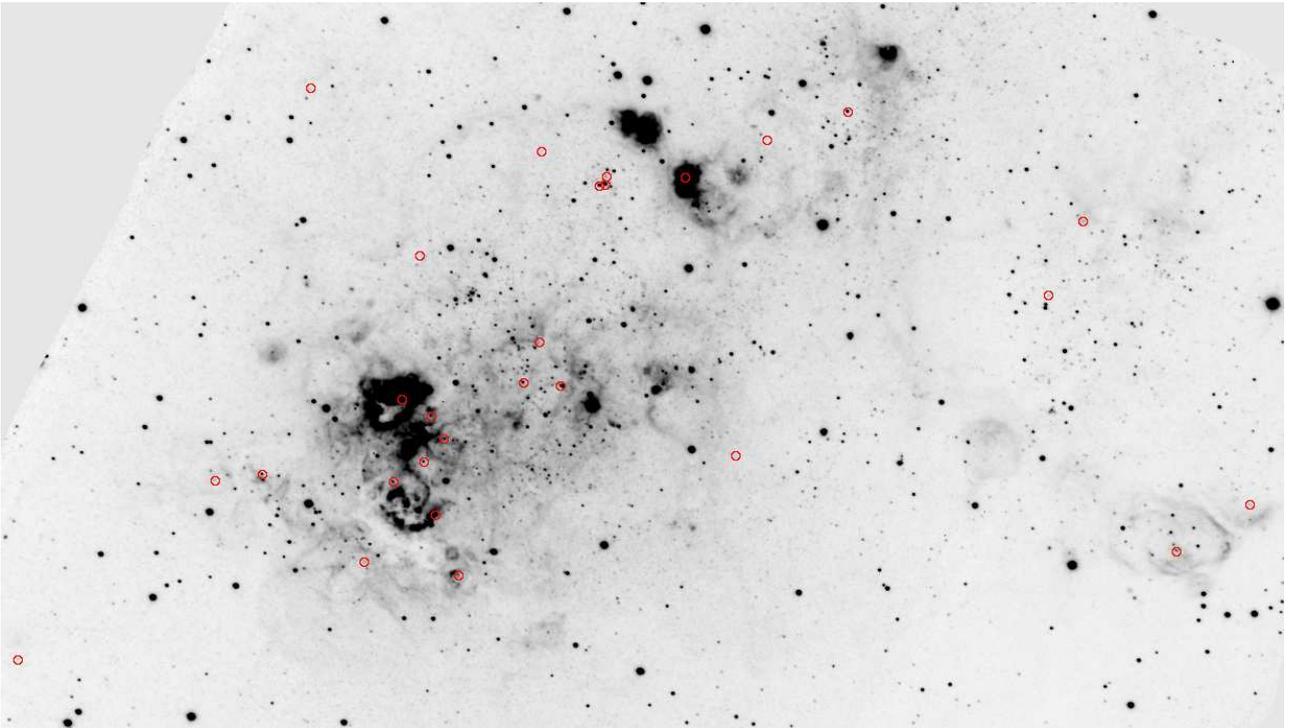
Figure 5. Gemini GMOS Hα image of IC10, north is up and east is left, showing the distribution of ionized gas and the relative positions of confirmed WR stars (red circles) with the exception of M5 which is out of the field of view but is associated with the H II region HL29. The bright star forming complex HL106/111 (left of centre) contains 6 WR stars. Field of view is $384'' \times 210''$, corresponding to 1.4×0.8 kpc at a distance of 740 kpc.

extinction is negligible, and therefore does not effect the measured radio flux. We do, however, note that contributions from non-thermal radio sources such as synchrotron emission from supernova remnants can skew results, especially at longer radio wavelengths. The radio SFRs shown from Gregory et al. (1996) and Chyży et al. (2016) have not been corrected for this contribution.

4   STELLAR RESULTS

4.1   New Wolf-Rayet Stars

The spectra of three newly confirmed WR stars in IC10 are presented in Fig. 6. All three have been assigned early WN (WNE) spectral types. Both T5 and T6 are associated with star clusters which is evident from both the photometry and the presence of a strong continuum. Also, as discussed in Sect. 3.2, T5 is located within the H II region HL45. Spectroscopy for T9 was also performed and analysis concluded that it was not a WR star. The presence of molecular TiO bands suggested it is most likely to be a foreground early M-dwarf star instead.

The number of spectroscopically confirmed WR stars in IC10 has increased from 26 to 29 stars, and a summary of their spectral properties can be found in Table 8. Of the previously confirmed WR stars, we suggest some changes to prior spectral classifications, including the revision of M15 from WC6-7 (Massey & Armandroff 1995) to WC4 due to the absence of C III 5696 and presence of O III 5592 shifting the equivalent width ratios outlined in Smith et al. (1990);

Crowther et al. (1998) into the WC4 category. The adjustment of M24 from a WNE/OB (Massey & Holmes 2002) to a O2.5 If/WN6 due to its similarity to HD93162 (Crowther & Walborn 2011). Finally, the minor adjustment to the subclass of M23 from WN7-8 (Massey & Holmes 2002) to WN7 based on the strengths of He I 5876 to He II 5411. Table 2 includes a complete census of the WR population and their classifications.

As mentioned previously, the WC/WN ratio in IC10 is peculiar, and since the addition of three new WN stars reduces the ratio from 1.3 to 1, IC10 is still regarded as an anomaly given the WC/WN ratio of $\sim$0.2 for the LMC and 0.1 for the SMC.

4.2   Binary Fraction

Recent evidence suggests the local OB binary frequency is high. Analysis of radial velocity variations in O-stars within the 30 Doradus region of the LMC by Sana et al. (2013) revealed a lower limit intrinsic binary fraction of $51 \pm 4\%$. Similarly, using O stars residing in Galactic clusters, Sana et al. (2012) found a lower limit binary fraction of $69 \pm 9\%$. Initial binary fractions for these regions most likely will have been higher but will have been disrupted over time.

If we assume a similar scenario for IC10, we would expect that some of these OB binaries would have survived the transition to WR stars, and therefore we expect a relatively high WR binary frequency. To assess this we outline a number of criteria used to identify potential binary candidates

Table 7. Comparison of the IC10 star formation rates derived using both radio flux measurements and Hα luminosity measurements, including a new attempt from this work. All values have been scaled to a distance of 740 kpc. Radio SFRs assume all flux measured is free-free radio emission and there is no contribution from non-thermal sources.

Method	ν [GHz]	F_λ [mJy]	$10^{-12}\,F_{H\alpha}$ [erg cm^{-2} s^{-1}]	$A_{H\alpha}$ [mag]	N II/Hα	$10^{39}\,L_{H\alpha}$ [erg s^{-1}]	SFR [M$_\odot$yr^{-1}]	Ref
Radio	4.85	137 ± 12					0.030 ± 0.003	a
Radio	1.43	377 ± 11					0.073 ± 0.005	b
Hα			103 ± 28	1.90	0.080 ± 0.008	3.89 ± 0.86	0.031 ± 0.007	c
Hα			130 ± 33	2.06 ± 0.49	0.092 ± 0.023	5.64 ± 2.93	0.045 ± 0.023	d

a: Gregory et al. (1996); b: Chyży et al. (2016); c: Kennicutt et al. (2008); d: This work
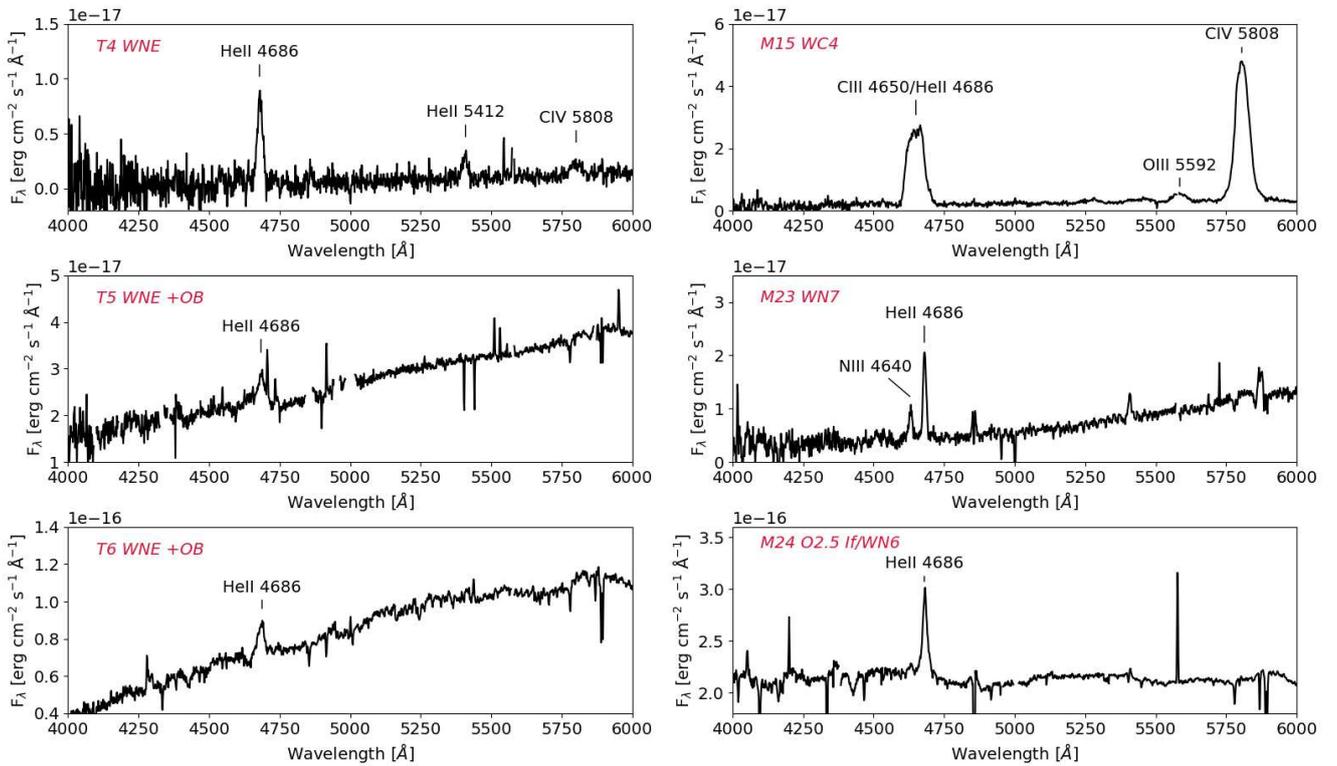
Figure 6. On the left we show the flux calibrated optical spectra of 3 newly confirmed WR stars within IC10, all belonging to the WN subclass. On the right we show the optical spectra for 3 previously confirmed WR stars, which were not included in the Gemini/GMOS datasets presented by Crowther et al. (2003) and therefore providing a complete set of spectra for all IC10 confirmed WR stars. Some nebular emission has been removed for clarity. The strong, broad absorption feature at λ4430 in T6 and M24 is a prominent Diffuse Interstellar Band (Herbig 1995).

and compare the resultant binary fraction with that of WR stars in other Local Group galaxies.

The simplest method involves identifying absorption features from OB companions in the spectrum of each WR star. There is however, some ambiguity in this approach, since WR stars may contain intrinsic absorption features, so alone this is insufficient to confidently suggest a binary system.

Another method involves searching for unusual radial velocities in the strongest emission line features present in the spectrum. Geocentric radial velocity measurements were found for those WR stars with nebular emission available, and heliocentric corrections were found for each mask using

the BCVcor task in IRAF. For those WR without nebular emission an average heliocentric radial velocity of -347 $\pm$ 75 kms^{-1} was assumed. This agrees well with the expected radial velocity of 348 $\pm$ 1 kms^{-1} (Huchra et al. 1999) and takes into consideration the average dispersion velocity of the gas, found to be 34 $\pm$ 5 kms^{-1} (McConnachie 2012). By measuring the radial velocity for He II 4686 (WN) and C IV 5808 (WC) emission lines in each spectrum and comparing with the expected radial velocity measurement, the WR stars with shift excesses greater than 2σ were identified as potential binary candidates or runaway stars.

Finally, the continuum of an O-star companion can also dilute the emission line strength of the WR, therefore

the presence of a companion would result in weak equivalent width measurements and small ΔHe II-He IIC excesses. These stars are easily identifiable in Fig. 7 (a) and (b), in which emission line widths are compared against line strengths in IC10 and Magellanic Clouds WN and WC stars respectively. It is however, important to note that nearby sources or line-of-sight contaminations can also enhance the continuum and falsely suggest a binary system.

Taking all these indicators into consideration, those WR stars which meet a minimum of two out of the three requirements were deemed likely to be part of a binary system, and have been indicated in Table 8, giving a coarse binary fraction of 41%. Of these potential binary systems, four WR stars (M1, M4, T5 and T6) successfully fulfilled all three of the binary system criteria. This estimated binary fraction is in good agreement with the observed WR binary fraction in both the LMC (Breysacher et al. 1999; Neugent et al. 2012a; Massey et al. 2014, 2015b) and SMC(Foellmi et al. 2003a), which again are lower limits, suggesting the mechanism for producing binaries is metallicity independent (Shenar et al. 2016).

4.3   Stellar Extinction

Interstellar extinction studies of IC10 have previously been attempted using H II regions, from which an E(B-V) = 0.83 $\pm$ 0.20 was obtained (Sect. 3.1). Here we derive new E(B-V) values of individual WR stars based on photometric magnitudes and spectral types. We consider the extinction in two continuum bands, He IIC at 478nm, and HαC at 662nm as follows:

$$E(\text{He IIC - H}\alpha\text{C}) = (\text{He IIC - H}\alpha\text{C}) - (\text{He IIC - H}\alpha\text{C})_0$$
$$= A_{\text{He IIC}} - A_{\text{H}\alpha\text{C}}$$

The conversion from reddening to E(B-V) was achieved using the Galactic extinction law (Seaton 1979). Assuming $R_\lambda = 3.1$ A_λ/E(B-V), ratios at wavelengths of 478nm(He IIC) and 662nm(HαC) were determined to be $A_{\text{He IIC}} = 3.7$ E(B-V) and $A_{\text{H}\alpha\text{C}} = 2.44$ E(B-V) respectively, resulting in:

$$E(B-V) = 0.79[(\text{He IIC - H}\alpha\text{C}) - (\text{He IIC - H}\alpha\text{C})_0]$$

Intrinsic He IIC-HαC values are dependent on WR subtype, therefore for each class, the He IIC and HαC magnitudes were determined from model spectra, free from extinction, to find the intrinsic colour. Where possible we used LMC template WR stars, however there are no late-type WC stars within the LMC so for this case we used a model for a Milky Way WC star. For cases where the WR spectra is dominated by OB stars we use Starburst99 population synthesis models at an age of 5Myr, since this is the typical age of stellar clusters hosting WR stars (Leitherer et al. 1999). Table C1 lists these results along with their associated model references.

Where possible we have attempted to derive individual extinction values tailored to each star. A comparison between the nebular and photometrically derived extinctions for T5 (HL45) gives E(B-V)=1.13 $\pm$ 0.04 and E(B-V)=1.15

$\pm$ 0.03 respectively, showing the two methods are in agreement. For the remainder of the sample, where robust magnitude measurements were unavailable, an average extinction value of E(B-V) = 0.92 $\pm$ 0.26 was applied, obtained from both the stellar extinction (E(B-V)=0.95 $\pm$ 0.27), and nebular extinction (E(B-V)=0.83 $\pm$ 0.20) results. The E(B-V) values applied for each star are included in Table 2.

4.4   WR Line Luminosities

Average WR emission line luminosities are very useful for interpreting extragalactic observations of young star forming regions. Significant WR populations can be found in distant galaxies which have recently undergone a burst of massive star formation, however individual WR stars will be unresolved. To probe the WR content we must rely on integrated WR emission line luminosities from the galaxy, calibrated using nearby resolved populations (Schaerer & Vacca 1998; Sidoli et al. 2006).

Here we present the average WR line luminosities obtained for IC10. We divide the WR population into five categories based on spectral type and determine the luminosities of the strongest emission lines associated with that WR class. The individual stellar extinctions applied for each star are shown in Table 2. Individual line luminosities can be found in Table 8 and the average results are summarised in Table 9. For comparison, we also include Magellanic Cloud WR line luminosity data taken from Crowther & Hadfield (2006). Fig. 8 provides a visual representation for the comparison of individual line luminosities between IC10 and Magellanic Cloud WN, WC and WO stars.

WN stars, using the He II 4686 emission line, appear to show conflicting results. For WN2-5 (WNE) stars the average line luminosity of 6.7 $\pm$ 6.0 $\times 10^{35}$ erg s^{-1} for IC10 is similar to LMC counterparts, whereas for WN6-9 (WNL) stars however, the IC10 average of 5.7 $\pm$ 3.4 $\times 10^{35}$ erg s^{-1} is somewhat lower than both the Magellanic Clouds. We note however, that the sole late WN star in the SMC is the unusual system HD5980 (Koenigsberger et al. 2014), and the LMC statistics include the hydrogen rich WN stars in 30 Doradus.

The similarities between IC10 and LMC WN stars can been seen in Fig. 8, while SMC WN stars can be seen to have lower luminosities than their LMC and IC10 counterparts.

WCE stars in IC10 and the LMC, which all belong to the WC4 class, have comparable C IV 5808 emission line averages, however there is no counterpart for the IC10 late WC (WCL) star in either of the Magellanic Clouds. This provides an opportunity to extend the local line luminosity calibrators to include WC7 stars at LMC metallicity. However, our WCL sample consists of only M10. Smith et al. (1990) find that Galactic late WC stars have lower C IV 5808 fluxes than WC4 stars, with an average emission line luminosity of 3.81 $\pm$ 0.46 $\times 10^{35}$ erg s^{-1}, therefore suggesting M10 is unusually luminous and may not be typical.

Table 8. Emission line properties of the strongest spectral features found in the confirmed WN and WC stars of IC10. Line luminosities derived using the individual interstellar extinction values outlined in Table 2 and discussed in Sect. 4.3, along with a distance of 740 ± 20 kpc. Mask column refers to the mask the star was observed through. Multiple masks indicate that the star was observed more than once, therefore these spectra were combined to improve signal to noise. For WN stars the strongest lines usually refer to He II 4686 and He II 5411 emission (with the exception of the WNE/C star M5). For WC stars the strongest features are C IV 5808 and, due to the broad nature of the emission lines, a C III 4650/He II 4686 blend. Binary column indicates stars that successfully met two out of the three binary criteria outlined in Sect. 4.2. Note this only suggests and does not confirm binary status of a star.

ID	Spectral Type	He II 4686				He II 5411				Mask	Radial Velocity	Binary
		FWHM [Å]	Log W_λ [Å]	10^{-17} f_λ [erg cm^{-2} s^{-1}]	10^{35} L_λ [erg s^{-1}]	FWHM [Å]	Log W_λ [Å]	10^{-17} f_λ [erg cm^{-2} s^{-1}]	10^{35} L_λ [erg s^{-1}]		[kms^{-1}]	
T4	WNE	23 ± 1	2.65 ± 0.02	19 ± 1	4.5 ± 1.6	22 ± 3	1.73 ± 0.05	5 ± 1	0.6 ± 0.2	1	-317	
R13	WN5	28 ± 1	2.19 ± 0.02	18 ± 1	1.9 ± 0.8	28 ± 3	1.66 ± 0.04	4 ± 0	0.3 ± 0.1	2,3	-80	
T5	WNE	32 ± 0	1.08 ± 0.03	20 ± 3	10.9 ± 3.2					1,2	-30	b?
R9	WNE	28 ± 1	1.67 ± 0.02	18 ± 1	2.0 ± 0.2	31 ± 3	0.98 ± 0.04	6 ± 1	0.4 ± 0.1	2,3	-222	
T6	WNE	27 ± 2	0.81 ± 0.03	46 ± 3	16.6 ± 2.1					1	-82	b?
R8	WN10	46 ± 5	1.19 ± 0.04	28 ± 2	2.9 ± 0.4					4	-19	b?
M9	WN3	31 ± 0	2.58 ± 0.01	47 ± 1	4.8 ± 0.9	29 ± 6	1.85 ± 0.07	9 ± 1	0.6 ± 0.1	3	-251	
R12	WNE	58 ± 3	2.13 ± 0.03	24 ± 1	16.7 ± 2.5					4	259	
M24	O2.5 If/WN6	21 ± 1	0.88 ± 0.01	163 ± 4	10.4 ± 1.1					2	-204	
R2	WN7-8	18 ± 0	1.62 ± 0.01	31 ± 1	5.9 ± 0.5	17 ± 4	0.79 ± 0.08	6 ± 1	0.6 ± 0.1	2,3	-117	b?
M17	WNE + BH	20 ± 4	1.01 ± 0.07	8 ± 1	1.2 ± 0.2					4		var.
M19	WN4	24 ± 1	2.07 ± 0.01	44 ± 1	1.8 ± 0.3	29 ± 1	1.52 ± 0.01	10 ± 0	0.3 ± 0.04	1,3,4	-260	
M23	WN7	13 ± 0	1.72 ± 0.01	23 ± 1	3.7 ± 3.3	12 ± 1	0.83 ± 0.04	6 ± 0	0.5 ± 0.4	2	-286	
M21	WN4	28 ± 0	2.38 ± 0.00	54 ± 1	7.0 ± 0.8	29 ± 1	1.66 ± 0.01	12 ± 0	0.9 ± 0.1	2,3	-117	
		C III 4650/He II 4686 blend				C IV 5808						
M5	WNE/C4	53 ± 1	2.53 ± 0.01	89 ± 2	21.8 ± 2.4	79 ± 1	3.09 ± 0.01	370 ± 6	38.4 ± 3.6	3,4	-422	
M1	WC4-5	65 ± 3	1.86 ± 0.02	46 ± 2	7.5 ± 6.8	51 ± 1	1.99 ± 0.01	84 ± 2	6.3 ± 4.3	4	239	b?
M2	WC4	69 ± 1	2.17 ± 0.01	138 ± 2	22.5 ± 20.3	63 ± 1	2.50 ± 0.01	322 ± 5	24.0 ± 16.4	2	-460	
R6	WC4	73 ± 2	2.29 ± 0.01	45 ± 1	25.9 ± 3.7	75 ± 1	2.41 ± 0.01	95 ± 2	18.4 ± 2.1	2,4	-158	b?
R5	WC4-5	74 ± 1	2.16 ± 0.01	64 ± 1	11.3 ± 1.6	72 ± 5	2.18 ± 0.03	99 ± 6	7.9 ± 1.0	2,4	-183	b?
M4	WC4-5	67 ± 1	1.65 ± 0.01	204 ± 3	32.9 ± 2.4	48 ± 1	1.53 ± 0.01	183 ± 4	13.6 ± 0.9	1	-163	b?
M7	WC4-5	81 ± 1	2.73 ± 0.01	836 ± 12	137 ± 123	79 ± 2	2.44 ± 0.01	1002 ± 27	75 ± 51	1	-205	
R11	WC4	83 ± 4		69 ± 4	11.3 ± 10.2	82 ± 1		274 ± 3	20.4 ± 14.0	1	-445	
M10	WC7	68 ± 0	3.06 ± 0.00	904 ± 7	496 ± 41.2	84 ± 1	3.06 ± 0.01	1128 ± 15	210 ± 15.8	4	-47	
M12	WC4	53 ± 2	1.96 ± 0.02	40 ± 2	80.9 ± 10.9	51 ± 1	1.87 ± 0.01	99 ± 2	49.1 ± 5.2	3	10	b?
R10	WC4	61 ± 2	3.39 ± 0.01	84 ± 2	13.7 ± 12.4	52 ± 1	3.13 ± 0.00	118 ± 1	8.8 ± 6.0	1	-279	
M13	WC5-6	59 ± 1	2.07 ± 0.01	161 ± 3	8.3 ± 0.7	48 ± 1	1.99 ± 0.01	163 ± 2	5.1 ± 0.4	4	-59	b?
M14	WC5	77 ± 1	2.64 ± 0.00	588 ± 6	115 ± 10.7	78 ± 1	2.51 ± 0.01	622 ± 9	53.1 ± 4.4	1,3	-32	b?
M15	WC4	65 ± 1	3.00 ± 0.01	180 ± 3	7.5 ± 1.8	55 ± 0	2.92 ± 0.00	269 ± 2	7.1 ± 1.3	1,2	-274	
M20	WC5	61 ± 0	2.94 ± 0.00	272 ± 2	39.2 ± 5.4	53 ± 1	2.82 ± 0.00	269 ± 3	18.2 ± 2.0	1,3	-232	

M17 is a known X-ray binary, involving a WR and black hole orbiting with a 34.93 ± 0.04 hr period. (Prestwich et al. 2007; Silverman & Filippenko 2008).

Table 9. Average line luminosities of the He II 4686, and C IV 5808 for the WN and WC/O spectral classes respectively. Both the WN and WC class have been further divided using ionization classifications into early and late subgroups. To avoid confusion, the WNE/C star M5 has not been included in any category. For comparison, the mean line luminosities obtained for the LMC and SMC have been included from Crowther & Hadfield (2006) data.

Spectral Type	Emission line [Å]	IC10		LMC		SMC	
		WR [#]	$L_\lambda \times 10^{35}$ [erg s^{-1}]	WR [#]	$L_\lambda \times 10^{35}$ [erg s^{-1}]	WR [#]	$L_\lambda \times 10^{35}$ [erg s^{-1}]
WN2-5 (WNE)	He II 4686	10	6.73 ± 6.00	45	9.27 ± 8.74	6	0.62 ± 0.32
WN6-9 (WNL)	He II 4686	4	5.71 ± 3.37	15	13.3 ± 15.2	1	7.79
WC4-6 (WCE)	C IV 5808	13	23.6 ± 21.8	17	32.5 ± 15.8		
WC7 (WCL)	C III 5696	1	87 ± 8				
WC7 (WCL)	C IV 5808	1	203 ± 18				
WO	C IV 5808			1	10.2	1	14.9
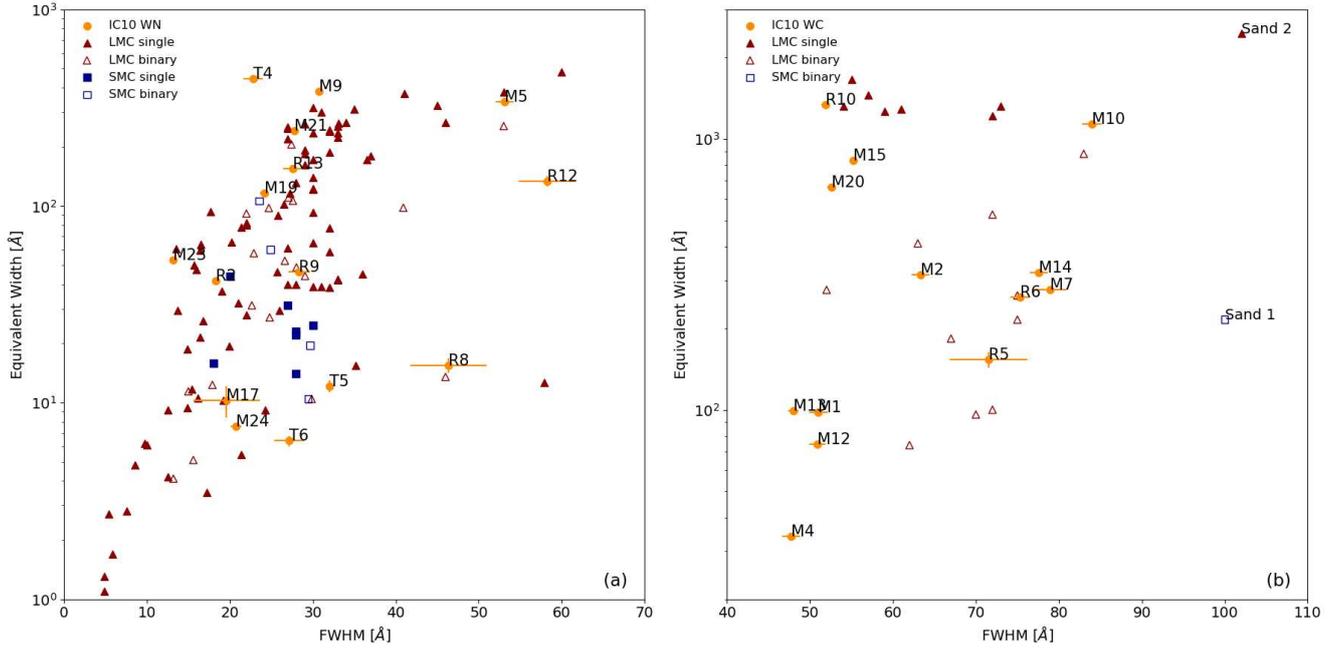
Figure 7. Shows the relationship between FWHM and equivalent width for (a) WN stars and (b) WC stars in the LMC (red triangles), SMC (blue squares), and IC10 (yellow circles). For the Magellanic cloud WR stars, binary and single stars can also be distinguished between by open and filled plot symbols respectively. The two known Magellanic WO stars have also been included (Sand 1,2). LMC data taken from Crowther & Hadfield (2006), Schnurr et al. (2008), and Foellmi et al. (2003b). SMC data from Foellmi et al. (2003a) and Crowther & Hadfield (2006).
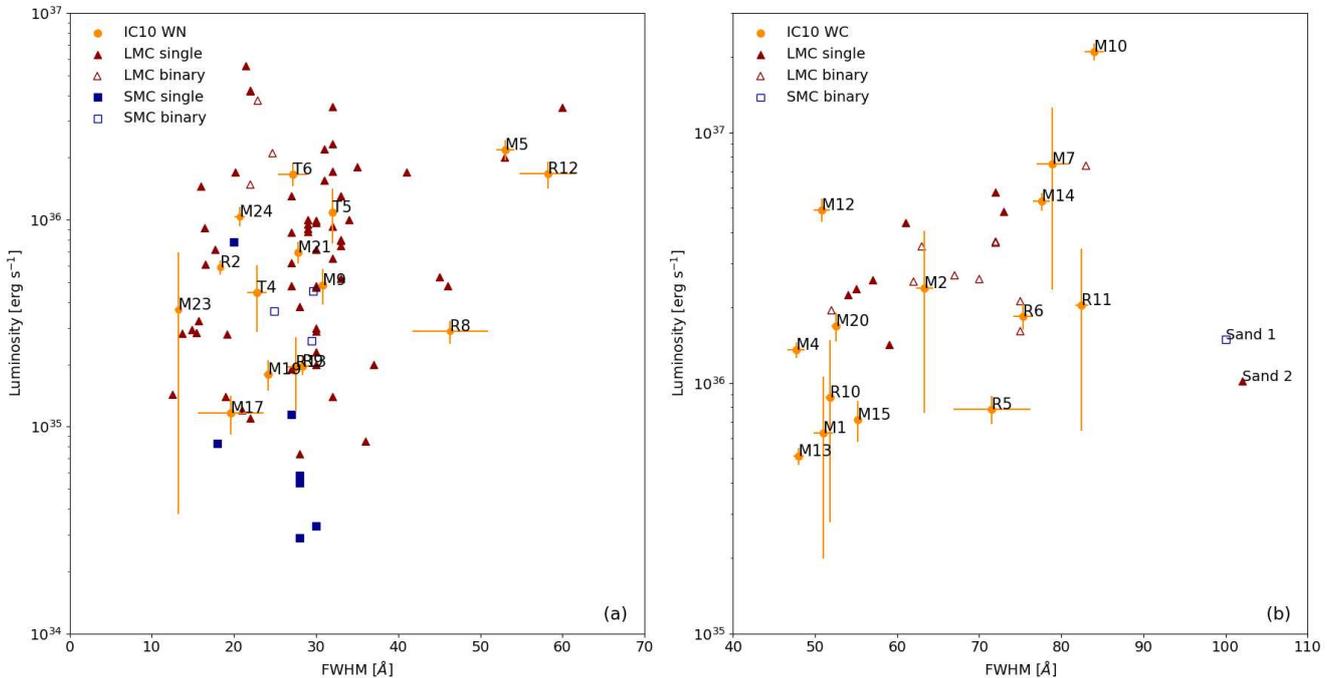
Figure 8. Shows the relationship between FWHM and line luminosity for (a) WN stars using the He II 4686 emission line, and (b) WC and WO stars using the C IV 5808 emission line. The corresponding host galaxy for each WR can be identified from plot symbol and colour using the following; LMC (red triangles), SMC (blue squares), and IC10 (yellow circles). For the Magellanic cloud WR stars, binary and single stars can also be distinguished between by open and filled plot symbols respectively. LMC data taken from Crowther & Hadfield (2006), Schnurr et al. (2008), and Foellmi et al. (2003b). SMC data from Foellmi et al. (2003a) and Crowther & Hadfield (2006).

5 DISCUSSION

5.1 WR Content

Table 10 provides a comparison between IC10 and Magellanic Cloud galactic properties. The size and low metallicity of IC10 has meant that it had previously been considered as a SMC-like galaxy, however when considering the revised metallicity, the presence of WC stars, and average line luminosity comparisons, IC10 bears closer resemblance to the LMC than the SMC.

The total number of spectroscopically confirmed WR stars in IC10 has increased to 29, with a WC/WN ratio of 1.0, putting aside the intermediate WN/C star M5. From Table 10, if we take the LMC WR content, which one can consider to be essentially complete (Massey et al. 2015b), and scale this to the IC10 SFR of 0.045 $M_\odot yr^{-1}$ we find the expected number of WR stars is ∼28, which agrees well with our result and suggests that the IC10 WR survey is also relatively complete.

The WC/WN ratio of IC10 is substantially higher than the LMC value of ∼0.2, suggesting an excess of WC stars. Deep imaging reveals a further 6 potential candidates, and if all 6 remaining candidates were confirmed as WN stars, the WC/WN ratio would fall again to 0.7.

Whilst we acknowledge that the method outlined here has limitations regarding the identification of WR stars located in dense local stellar environments, we consider this survey near complete. It should also be noted that a recent survey of the LMC has identified weak emission line WN3 stars, with characteristically faint magnitudes of -2.5 ± 0.5 mag (Massey et al. 2014, 2015b). The He IIC sensitivity limit of our survey however is -2.4 mag for a 3σ detection, which should be sufficient to identify some of the faint stars belonging to this class. Considering these faint WN3 +abs stars comprise ∼ 6% of the LMC WR population, we are confident a huge hidden population of WR stars does not remain undiscovered within IC10.

5.2 WC/WN Ratio

The evolution of WR stars from the WN phase to the WC phase is due to mass loss, which is primarily dictated by metal-driven winds, as seen in the clear trend of increasing WC/WN ratio with metallicity in the Local Group (Massey et al. 2015a; Crowther 2007). For IC10 however, with an LMC-like metallicity, the high WC/WN ratio remains peculiar, suggesting this relationship also depends on another parameter. From Table 10 we see than the SFR in IC10 is unremarkable, however the star formation surface density (Σ_{SFR}) far exceeds those of the Magellanic Clouds. We therefore consider the Σ_{SFR} as a second parameter in our understanding of WC/WN ratios.

Massive stars are generally formed in clusters (Portegies Zwart et al. 2010), for which it is known from the cluster mass function that high mass clusters are rare and low mass clusters are common (Whitmore et al. 1999; Zhang & Fall 1999). Increasing the star formation intensity extends the cluster mass function to higher masses, such that the truncation of the upper cluster mass increases for starburst regions with respect to their quiescent star forming counterparts (Gieles 2009). A second relationship exists between cluster mass and its most massive star, proposed by Weidner & Kroupa (2006). Combining these two results allows us to draw the conclusion that regions of more intense star formation are capable of producing higher mass stars, fully sampling the IMF, whereas quiescent star forming regions would exhibit a deficit of high mass stars. This result is significant because the initial mass of the O-star can play a crucial role in the future evolution of the WR star through the WN and WC phases.

When observing LMC WN stars, Hainich et al. (2014) found that the stellar evolution tracks modelled using the Geneva group stellar evolution models (Meynet & Maeder 2005) show the majority of WN stars had initial masses within the range of 25-40 $M_\odot$. Meanwhile the progenitors of LMC WC stars are likely to have had initial masses greater than 40$M_\odot$(Crowther et al. 2002; Meynet & Maeder 2005). Therefore larger initial masses are required for single stars to progress to the WC stage.

Comparing IC10 to the LMC, with similar host metallicity environments, we see the global SFR of IC10 is lower but the star formation surface density is an order of magnitude higher (see Table 10). The high Σ_{SFR} will extend the stellar mass limit to higher masses, in turn increasing the frequency of higher mass stars. If IC10 has been host to a higher proportion of massive O-stars, the percentage of WR stars capable of achieving the mass-loss rates necessary to reach the WC phase would also increase and the WC/WN ratio would rise to reflect this, as is observed. Indeed, the WC/WN ratio of the dominant star-forming complex of IC10, comprising of HL106/111 (Hodge & Lee 1990) is especially high, as summarised in Table 10.

Within the Local Group, the closest analogue to the high Σ_{SFR} of IC10 is the 30 Doradus region in the LMC. A census of the WR content of 30 Doradus, within 15′of R136, implies a ratio of WC/WN = 0.25 (Breysacher et al. 1999; Doran et al. 2013). However, putting aside main sequence very massive WN5h(a) stars, the WC/WN ratio rises to 0.42. Again, this increased ratio arises from the high Σ_{SFR} of 30 Doradus, leading to an increased frequency of high mass stars in this region and consequently a higher WC/WN ratio. Similarly, a low Σ_{SFR} at high metallicity would produce a low WC/WN ratio. By way of example, the super-solar metallicity galaxy M31 has a relatively low Σ_{SFR} and a modest WC/WN = 0.67 ratio (Neugent et al. 2012b).

6 CONCLUSION

Our main results can be summarized as follows:

(i) Using deep narrow-band imaging to search for a He II 4686 magnitude excess, we present 11 WR candidates in IC10 and spectroscopically confirm 3 of these as WN stars, whilst rejecting 1 as an early M-dwarf and suggesting another is unlikely to be a WR star due to the dispersed nature of the source. The total number of WR stars in IC10 has now been raised from 26 to 29, and the WC/WN ratio has lowered to 1.0. We review previous spectral classifications and suggest updates for 3 previously confirmed WR stars, M15, M23 and M24.

(ii) An updated SFR measurement of 0.045 ± 0.023 $M_\odot yr^{-1}$ has been derived from Hα luminosity, an increase from the previous result of 0.031 ± 0.007 (Kennicutt et al.

Table 10. Comparing galactic and individual star forming region properties of Local Group members with similar metallicity to IC10. Distances to the LMC and SMC were taken as 50kpc and 60kpc respectively (Westerlund 1990). 30 Dor. refers to the 30 Doradus star forming region within the LMC, HL 111/106 refers to the central star forming region of IC10. Bracketed values reflect potential changes to the WR number and WC/WN ratio in IC10 should all 6 potential WR candidates be successfully confirmed as WN stars.

Galaxy	Distance [kpc]	Log $\frac{O}{H}$+12	Ref	10^{39} $L_{H\alpha}$ [erg s^{-1}]	SFR [M$_\odot$yr^{-1}]	Ref	R$_{25}$ [']	Σ_{SFR} [M$_\odot$yr^{-1} kpc^{-2}]	Ref	WR [#]	WC/WN [#]	Binary Fraction [%]	Ref
LMC	50	8.37	a	31	0.260	c	646	0.0036	e,f	154	0.19	29	g,h,i,j
SMC	60	8.13	a	4.68	0.046	c	316	0.0016	e	12	0.1	42	k
IC10	740	8.40	b	5.64	0.045	b	6.3	0.049	e	29	1	41:	b
										(35)	(0.7)		
30 Dor.	(LMC)			14	0.108	d	15*	0.722	d	27	0.25	20	l
HL 111/106	(IC10)			1.44	0.011	b	0.30×0.46*	0.559	b	6	2	67	b

a: Garnett (1990); b: this work; c: Kennicutt et al. (2008); d: Kennicutt et al. (1995); e: Crowther & Bibby (2009); f: de Vaucouleurs et al. (1991) g: Breysacher et al. (1999); h: Neugent et al. (2012a); i: Massey et al. (2014); j: Massey et al. (2015b); k: Foellmi et al. (2003a); l: Doran et al. (2013);
*R$_{25}$ radius used for all galaxies (de Vaucouleurs et al. 1991) excluding 30 Doradus (Kennicutt et al. 1995) and the ellipse used for HL 111/106 complex.
The colon following the binary fraction highlights the uncertainty in this measurement since a robust method has not been used to confirm potential binary candidates.

2008). This updated Hα SFR is intermediate between radio derived SFRs, however we note the radio fluxes have not been corrected to eliminate non-thermal radio sources.

(iii) Using nebular emission from the H II region HL45, associated with the WR star T5, the oxygen abundance for IC10 has also been updated from 8.26 to 8.40 ± 0.04, suggesting IC10 has an LMC-like metallicity. Comparison of emission line luminosities also revealed similar results for WNE and WCE stars in IC10 and the LMC, emphasising the similarities, however the WNL and WCL results were less consistent, most likely due to the small number of stars in these categories.

(iv) The WC/WN ratio observed for IC10 remains peculiar, despite the potential addition of our 6 new unconfirmed candidates. We propose the most likely explanation is due to the high star formation surface density of the galaxy, which extends the cluster upper stellar mass limit to higher values. Assuming the WC initial mass limit is higher than for WN stars, the higher WC/WN ratio observed in IC10 would be expected as a result of the higher star formation intensity observed in this galaxy.

REFERENCES

Breysacher J., Azzopardi M., Testor G., 1999, A&AS, 137, 117
Cairós L. M., Caon N., Weilbacher P. M., 2015, A&A, 577, A21
Chambers K. C., et al., 2016, preprint, (arXiv:1612.05560)
Chyży K. T., Drzazga R. T., Beck R., Urbanik M., Heesen V., Bomans D. J., 2016, ApJ, 819, 39
Crowther P. A., 2007, ARA&A, 45, 177
Crowther P. A., Bibby J. L., 2009, A&A, 499, 455
Crowther P. A., Hadfield L. J., 2006, A&A, 449, 711
Crowther P. A., Walborn N. R., 2011, MNRAS, 416, 1311
Crowther P. A., De Marco O., Barlow M. J., 1998, MNRAS, 296, 367
Crowther P. A., Dessart L., Hillier D. J., Abbott J. B., Fullerton A. W., 2002, A&A, 392, 653
Crowther P. A., Drissen L., Abbott J. B., Royer P., Smartt S. J., 2003, A&A, 404, 483
Dessart L., Crowther P. A., Hillier D. J., Willis A. J., Morris P. W., van der Hucht K. A., 2000, MNRAS, 315, 407
Doran E. I., et al., 2013, A&A, 558, A134
Foellmi C., Moffat A. F. J., Guerrero M. A., 2003a, MNRAS, 338, 360
Foellmi C., Moffat A. F. J., Guerrero M. A., 2003b, MNRAS, 338, 1025

García-Lorenzo B., Cairós L. M., Caon N., Monreal-Ibero A., Kehrig C., 2008, ApJ, 677, 201

Garnett D. R., 1990, ApJ, 363, 142

Gieles M., 2009, MNRAS, 394, 2113

Gonçalves D. R., Teodorescu A. M., Alves-Brito A., Méndez R. H., Magrini L., 2012, MNRAS, 425, 2557

González Delgado R. M., Leitherer C., Heckman T. M., 1999, ApJS, 125, 489

Gregory P. C., Scott W. K., Douglas K., Condon J. J., 1996, ApJS, 103, 427

Hainich R., et al., 2014, A&A, 565, A27

Herbig G. H., 1995, ARA&A, 33, 19

Hodge P., Lee M. G., 1990, PASP, 102, 26

Hook I. M., Jørgensen I., Allington-Smith J. R., Davies R. L., Metcalfe N., Murowinski R. G., Crampton D., 2004, PASP, 116, 425

Huchra J. P., Vogeley M. S., Geller M. J., 1999, ApJS, 121, 287

Kennicutt Jr. R. C., 1988, ApJ, 334, 144

Kennicutt Jr. R. C., 1998, ApJ, 498, 541

Kennicutt Jr. R. C., Bresolin F., Bomans D. J., Bothun G. D., Thompson I. B., 1995, AJ, 109, 594

Kennicutt Jr. R. C., Lee J. C., Funes J. G., J. S., Sakai S., Akiyama S., 2008, ApJS, 178, 247

Koenigsberger G., Morrell N., Hillier D. J., Gamen R., Schneider F. R. N., González-Jiménez N., Langer N., Barbá R., 2014, AJ, 148, 62

Leitherer C., et al., 1999, ApJS, 123, 3

Lequeux J., Peimbert M., Rayo J. F., Serrano A., Torres-Peimbert S., 1979, A&A, 80, 155

Massey P., Armandroff T., 1995, AJ, 109, 2470

Massey P., Holmes S., 2002, ApJL, 580, L35

Massey P., Armandroff T. E., Conti P. S., 1992, AJ, 103, 1159

Massey P., Neugent K. F., Morrell N., Hillier D. J., 2014, ApJ, 788, 83

Massey P., Neugent K. F., Morrell N. I., 2015a, in Hamann W.-R., Sander A., Todt H., eds, Wolf-Rayet Stars: Proceedings of an International Workshop held in Potsdam, Germany, 1–5 June 2015. Edited by Wolf-Rainer Hamann, Andreas Sander, Helge Todt. Universitätsverlag Potsdam, 2015., p.35-42. pp 35–42 (arXiv:1507.07297)

Massey P., Neugent K. F., Morrell N., 2015b, ApJ, 807, 81

McConnachie A. W., 2012, AJ, 144, 4

Meynet G., Maeder A., 2005, A&A, 429, 581

Neugent K. F., Massey P., Morrell N., 2012a, AJ, 144, 162

Neugent K. F., Massey P., Georgy C., 2012b, ApJ, 759, 11

Neugent K. F., Massey P., Hillier D. J., Morrell N. I., 2017, preprint, (arXiv:1704.05497)

Pettini M., Pagel B. E. J., 2004, MNRAS, 348, L59

Portegies Zwart S. F., McMillan S. L. W., Gieles M., 2010, ARA&A, 48, 431

Prestwich A. H., et al., 2007, ApJL, 669, L21

Richer M. G., et al., 2001, A&A, 370, 34

Royer P., Smartt S. J., Manfroid J., Vreux J.-M., 2001, A&A, 366, L1

Sana H., et al., 2012, Science, 337, 444

Sana H., et al., 2013, A&A, 550, A107

Sanna N., et al., 2008, ApJL, 688, L69

Schaerer D., Vacca W. D., 1998, ApJ, 497, 618

Schlafly E. F., Finkbeiner D. P., 2011, ApJ, 737, 103

Schnurr O., Moffat A. F. J., St-Louis N., Morrell N. I., Guerrero M. A., 2008, MNRAS, 389, 806

Seaton M. J., 1979, MNRAS, 187, 73

Shenar T., et al., 2016, preprint, (arXiv:1604.01022)

Shi F., Kong X., Li C., Cheng F. Z., 2005, A&A, 437, 849

Sidoli F., Smith L. J., Crowther P. A., 2006, MNRAS, 370, 799

Silverman J. M., Filippenko A. V., 2008, ApJ, 678, L17

Smartt S. J., Crowther P. A., Dufton P. L., Lennon D. J., Kudritzki R. P., Herrero A., McCarthy J. K., Bresolin F., 2001, MNRAS, 325, 257

Smith L. F., Shara M. M., Moffat A. F. J., 1990, ApJ, 358, 229

Smith L. F., Shara M. M., Moffat A. F. J., 1996, MNRAS, 281, 163

Stetson P. B., 1987, PASP, 99, 191

Tully R. B., et al., 2013, AJ, 146, 86

Weidner C., Kroupa P., 2006, MNRAS, 365, 1333

Westerlund B. E., 1990, A&A Rev., 2, 29

Whitmore B. C., Zhang Q., Leitherer C., Fall S. M., Schweizer F., Miller B. W., 1999, AJ, 118, 1551

Wilcots E. M., Miller B. W., 1998, AJ, 116, 2363

Zhang Q., Fall S. M., 1999, ApJ, 527, L81

de Vaucouleurs G., de Vaucouleurs A., Corwin Jr. H. G., Buta R. J., Paturel G., Fouqué P., 1991, Third Reference Catalogue of Bright Galaxies. Volume I: Explanations and references. Volume II: Data for galaxies between 0^h and 12^h. Volume III: Data for galaxies between 12^h and 24^h.

APPENDIX A: CANDIDATE WR STARS

APPENDIX B: BALMER EMISSION LINE STRENGTHS

APPENDIX C: MODEL WR INTRINSIC COLOURS

This paper has been typeset from a TEX/LATEX file prepared by the author.

Table A1. He II 4686 emission candidates identified from GMOS He II and He IIC filter images, using blinking and subtraction techniques to search for He II excesses. Candidates listed in increasing RA order.

ID	RA [J2000]	Dec	He II [mag]	He IIC [mag]	Hα [mag]	HαC [mag]	g [mag]	Δ He II-He IIC [mag]	Status
T1	00:20:04.54	59:18:05.4	24.119 ± 0.030	24.983 ± 0.035	22.312 ± 0.060	23.621 ± 0.117	24.213 ± 0.091	-0.86 ± 0.05	
T2	00:20:05.60	59:19:45.7	24.312 ± 0.036	24.633 ± 0.053			24.476 ± 0.168	-0.32 ± 0.06	
T3	00:20:06.99	59:17:47.1	24.211 ± 0.028	25.521 ± 0.053	22.406 ± 0.055		24.489 ± 0.162	-1.31 ± 0.06	
T4	00:20:14.47	59:18:49.9	23.249 ± 0.016	24.612 ± 0.034	22.765 ± 0.123	23.377 ± 0.121	23.958 ± 0.093	-1.36 ± 0.04	WNE
T5	00:20:17.43	59:18:39.2	21.054 ± 0.044	20.918 ± 0.054		19.532 ± 0.069		0.14 ± 0.07	WNE
T6	00:20:20.34	59:18:37.3	19.939 ± 0.019	19.801 ± 0.027	18.125 ± 0.022	18.561 ± 0.018	19.222 ± 0.018	0.14 ± 0.03	WNE
T7	00:20:23.35	59:17:31.2	23.098 ± 0.027	23.530 ± 0.065		22.205 ± 0.064	22.231 ± 0.037	-0.43 ± 0.07	
T8	00:20:27.70	59:19:15.1	24.671 ± 0.056	25.487 ± 0.059				-0.82 ± 0.08	extended
T9	00:20:32.74	59:15:46.4	22.570 ± 0.011	22.537 ± 0.008	19.214 ± 0.011	19.931 ± 0.012	21.635 ± 0.011	0.03 ± 0.01	non WR
T10	00:20:32.98	59:18:24.1	24.373 ± 0.042	25.111 ± 0.077		23.467 ± 0.089		-0.74 ± 0.09	
T11	00:20:35.90	59:18:49.8	23.055 ± 0.019	23.428 ± 0.022	21.894 ± 0.060	22.888 ± 0.088		-0.37 ± 0.03	

Table B1. Balmer emission line equivalent widths for the H II regions outlined in Sect. 3.1. As before, HL# refer to H II regions outlined by Hodge & Lee (1990) and H II# refer to candidate H II regions suggested by Royer et al. (2001).

Nebular Region	Mask	Log $W_{H\gamma}$ [Å]	Log $W_{H\beta}$ [Å]	Log $W_{H\alpha}$ [Å]
HL 6	2		0.469 ± 0.067	1.205 ± 0.006
HL 10	2		1.043 ± 0.034	1.759 ± 0.004
HL 20	3		0.960 ± 0.020	1.773 ± 0.004
HL 22	4		1.988 ± 0.004	2.685 ± 0.003
HL 45	3		1.940 ± 0.010	>3.00
HL 45	1	1.613 ± 0.004	2.176 ± 0.006	
H II 04	4		0.952 ± 0.014	1.661 ± 0.023
H II 07	3		2.654 ± 0.006	3.248 ± 0.002
H II 07	4		2.892 ± 0.012	3.521 ± 0.002
H II 08	3		2.565 ± 0.002	3.447 ± 0.002
H II 08	4	2.407 ± 0.006	2.695 ± 0.006	
H II 11	3		>3.00	

RA and DEC (J2000) co-ordinates for Royer et al. (2001) H II regions as follows: H II 04 (00:20:15.48, +59:18:40.6) H II 07 (00:20:18.51, +59:17:40.4) H II 08 (00:20:24.41, +59:16:55.2) H II 11 (00:20:19.36, +59:18:02.9)

Table C1. The $(\text{He IIC-H}\alpha\text{C})_0$ intrinsic colour of WR stars for different ionization subclasses, determined from the spectral model indicated by the reference column.

Spectral type	Template Star	$(\text{He IIC-H}\alpha\text{C})_0$	Ref
WN3-4	LMC-AB9	-0.06	a
WN6	HD 38282	0.03	a
WN7	HDE 269883	-0.01	a
WN8	LMC-AB11	0.00	a
WN10	BE 294	0.12	a
WC4-5	HD 37026	-0.05	b
WC6	HD 97809	-0.06	c
WC7	HD 156385	0.00	d
WR +OB		-0.21	e

a: Doran et al. (2013); b: Crowther et al. (2002); c: Smartt et al. (2001); d: Dessart et al. (2000); e: Leitherer et al. (1999)